Characterization of the [4Fe-4S]$^+$ Cluster at the Active Site of Aconitase by ^{57}Fe, ^{33}S, and ^{14}N Electron Nuclear Double Resonance Spectroscopy†

Melanie M. Werst,‡ Mary Claire Kennedy,§ Andrew L. P. Houseman,‡ Helmut Beinert,*,§,∥ and Brian M. Hoffman*,‡

Department of Chemistry, Northwestern University, Evanston, Illinois 60208, and Department of Biochemistry and National Biomedical ESR Center, Medical College of Wisconsin, Milwaukee, Wisconsin 53226

Received January 31, 1990; Revised Manuscript Received June 22, 1990

ABSTRACT: ^{57}Fe, ^{33}S, and ^{14}N electron nuclear double resonance (ENDOR) studies have been performed to characterize the [4Fe-4S]$^+$ cluster at the active site of aconitase. Q-band ^{57}Fe ENDOR of isotopically enriched enzyme, both substrate free and in the enzyme–substrate complex, reveals four inequivalent iron sites. In agreement with Mössbauer studies [Kent et al. (1985) *J. Biol. Chem. 260*, 6371–6881], one of the iron ions, Fe_a, which is easily removed by oxidation to yield the [3Fe-4S]$^+$ cluster of inactive aconitase, shows a dramatic change in the presence of substrate. The remaining iron sites, $Fe_{b1,2,3}$, show minor changes when substrate is bound. Methods devised by us for analyzing and simulating ENDOR spectra of a randomly oriented paramagnet have been used to determine the principal values and orientation relative to the g tensor for the hyperfine tensors of three of the four inequivalent iron sites of the [4Fe-4S]$^+$ cluster, Fe_a, Fe_{b2}, and Fe_{b3}, in the substrate-free enzyme and the enzyme–substrate complex. The full tensor for the fourth site, Fe_{b1}, could not be obtained because its signal is seen only over a limited range of the EPR envelope. ^{33}S ENDOR data for the enzyme–substrate complex using enzyme reconstituted with ^{33}S show that the four inorganic bridging sulfide ions of the [4Fe-4S]$^+$ cube have isotropic hyperfine couplings of $A(S) < 12$ MHz, and analysis indicates that they can be divided into two pairs, one with couplings of $A(S1) \lesssim 1$ MHz and the other with $A(S2) \sim 6$–12 MHz; the analysis further places these pairs within the cube relative to the iron sites. ^{33}S data for substrate-free enzyme is qualitatively similar and can be completely simulated by two types of S^{2-} ion, with $A(S1) \sim 7.5$ and $A(S2) \sim 9$ MHz; the full hyperfine tensors have been determined. The hyperfine values for the two enzyme forms correspond to surprisingly small unpaired spin density on S^{2-}. ^{14}N ENDOR at Q-band reveals a nitrogen signal that does not change upon substrate binding.

The accompanying paper (Werst et al., 1990) has reported on the characterization by ^{17}O, ^{1}H, and ^{2}H ENDOR spectroscopy of solvent, substrate, and inhibitor binding at the [4Fe-4S]$^+$ cluster of aconitase [citrate (isocitrate) hydro-lyase, EC 4.2.1.3]. The present paper presents information obtained by the same approach using the isotopes ^{57}Fe, ^{33}S, and ^{14}N. For general remarks on properties of the enzyme, we refer to the preceding paper. Concentrating here on the constituents of the cluster, we add the following.

The binding of substrate produces a localized Fe^{2+} state at Fe_a of the cluster. The other sites, labeled Fe_b, show minor changes due to substrate binding. Mössbauer spectroscopy of the reduced paramagnetic [4Fe-4S]$^+$ cluster with bound substrate shows hyperfine interaction from three types of iron sites, the Fe_a site and two types of Fe_b sites, the latter present in the ratio 2:1. Reduced aconitase in the absence of substrate could not be easily studied by Mössbauer because samples of the required purity could not be prepared. However, some preliminary results have been reported (Kent et al., 1985).

We have prepared ^{57}Fe-, ^{33}S-, and ^{77}Se-enriched enzyme (Figure 1) and have performed Q-band (35-GHz) ENDOR measurements to characterize the [4Fe-4S]$^+$ cluster forms of aconitase. These ^{57}Fe measurements could not have been performed in a standard, X-band (9-GHz) ENDOR spectrometer because the signals appear at radio frequencies of 8–24 MHz and suffer interference from strongly overlapping ^{1}H ENDOR centered at $\nu_H \sim 14$ MHz ($g \sim 2$). However, an increase of microwave frequency from 9 GHz (X-band) to 35 GHz (Q-band) shifts the center of the proton pattern to $\nu_H \sim 53$ MHz ($g \sim 2$) and eliminates the overlap of ^{1}H and ^{57}Fe signals.

Activation and exchange reactions have been used to isotopically label iron subsites of the [4Fe-4S]$^+$ cluster with $I = {}^1/_2$ ^{57}Fe in either the Fe_a site or the three complementary Fe_b sites. ^{57}Fe ENDOR and Mössbauer spectroscopies (Kent et al., 1985) agree that Fe_a experiences a pronounced change upon binding of substrate, whereas the remaining inequivalent iron sites, $Fe_{b1,2,3}$, show only minor changes. Detailed simulations of ENDOR spectra obtained at selected g values across the EPR envelope have allowed us to derive the principal values and orientation with respect to the g tensor of the hyperfine tensors for three of the four Fe sites of the [4Fe-4S]$^+$ cluster (Fe_a, $Fe_{b2,3}$) of the substrate-free enzyme and enzyme–substrate complex.

^{33}S ENDOR studies of the [4Fe-4S]$^+$ cluster of the isotopically enriched enzyme complexed with substrate show that the four bridging sulfide ions have hyperfine coupling constants $A(S) < 12$ MHz, and analysis indicates that they can be divided into two pairs, one pair with substantial hyperfine couplings and the other with hyperfine couplings close to zero. Their placement relative to the iron sites within the cluster cube is further determined. Likewise, ^{33}S ENDOR studies of the isotopically enriched [4Fe-4S]$^+$ substrate-free enzyme indicate that the four bridging sulfide ions are of two types and have hyperfine coupling constants $A(S) < 13$ MHz. Full simulations and analysis of these ^{33}S spectra are presented.

† This work was supported by the National Institutes of Health (GM 34812 to H.B. and HL 13531 to B.M.H.) and the National Science Foundation (DBM-8907559 to B.M.H.).

‡ Northwestern University.

§ Department of Biochemistry, Medical College of Wisconsin.

∥ National Biomedical ESR Center, Medical College of Wisconsin.

0006-2960/90/0429-10533$02.50/0

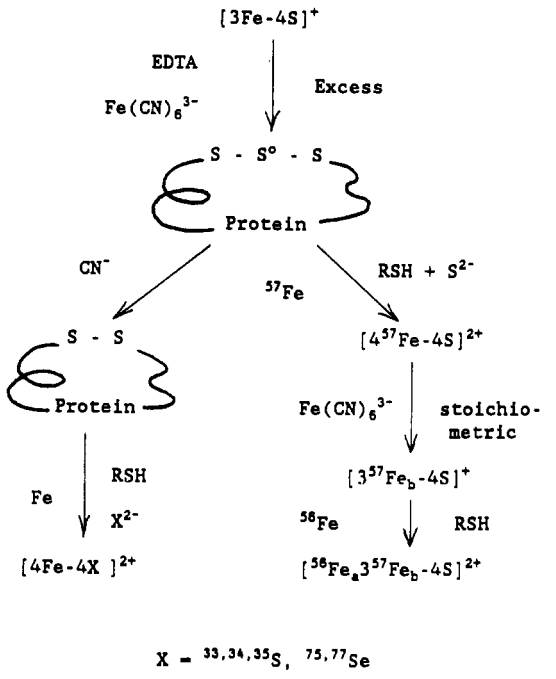

FIGURE 1: Scheme illustrating the preparation of specifically labeled Fe-S protein.

The reduced $[4Fe\text{-}4S]^+$ enzyme with natural isotopic abundance shows an ^{14}N signal that does not change upon substrate binding. ^{77}Se resonances have not been observed from reconstituted protein because of apparent interference from the ^{14}N resonances.

Procedures and Theory

Sample Preparation. Materials and methods were as previously reported in the accompanying paper (Werst et al., 1990) except where specifically described. Elemental ^{33}S, 99.23 atom %, was obtained from Alfred Hempel GMBH and Co., Düsseldorf, West Germany. Elemental ^{77}Se, 92.4 atom %, was obtained through Icon Services, Summit, NJ, and $Na_2{}^{75}SeO_3$ from ICN Radiochemicals, Irvine, CA. Reconstitution of apoprotein with Fe isotopes was modified as follows: the amount of Fe^{2+} and S^{2-} used is 8 and 6 times the molar concentration of enzyme, and the incubation time has been increased to ≥16 h. When apoenzyme was to be reconstituted with S or Se isotopes, cyanolysis to remove S^0 had to be performed. Apoenzyme in 0.1 M Hepes, pH 7.5, hereafter called buffer, was made 50 mM in NaCN by the addition of the appropriate amount of 0.5 M NaCN, and the pH was adjusted to 8.5–9.0 by the addition of 1 M Tris, pH 9.4. The solution was incubated in an ice bath for ≥2 h and desalted on G-50 columns equilibrated with buffer. Reconstitution with Fe^{2+} and S^{2-} isotopes was accomplished by using 8.0 times the molar concentration of enzyme for both Fe^{2+} and S^{2-}. $Na_2{}^{33,34}S$ was prepared from elemental sulfur by reduction with Na metal in liquid NH_3 (Brauer, 1963). Na_2SeO_3 was prepared from elemental selenium by oxidation of a weighed amount with concentrated HNO_3, evaporation of HNO_3, and dissolution of the white residue in 0.5 M NaOH to pH 7. Reconstitution was as previously described (Surerus et al., 1989). Anaerobic procedures were used whenever active enzyme was involved.

ENDOR Measurements. ENDOR spectra are recorded as described in the accompanying (Werst et al., 1990) and previous papers (Venters et al., 1986; Gurbiel et al., 1989). For use below, we recall that for a single-crystal ENDOR measurement from a nucleus (or set of equivalent nuclei) J of spin I one expects $4I$ transitions (selection rules, $\Delta m_s = 0$, $\Delta m_I = \pm 1$) having first-order transition frequencies given by (Abragam & Bleaney, 1970)

$$\nu_{\pm}(m_I) = |\pm A^J/2 + \nu_J + 3P^J(2m_I - 1)| \qquad (1)$$

where $-I + 1 \leq m \leq I$ and A^J and P^J are the angle-dependent hyperfine coupling and quadrupole tensors, respectively. In particular, the spectrum for ^{57}Fe ($I = {}^1/_2$) consists of a Larmor-split doublet centered at $A^{Fe}/2$ and with the ν_- and ν_+ signals separated by twice the Larmor frequency, $2\nu_{Fe}$, whereas a set of magnetically equivalent protons give a pair of ENDOR transitions, $\nu_{\pm}$, centered at the free proton Larmor frequency:

$$\nu_{\pm} = \nu_H \pm A^H/2 \qquad (2)$$

$\nu_H = (gH\beta_n/\beta_e)[\nu(M)/g_{obs}]$, which varies with the EPR spectrometer frequency and split by A^H. Simulations of spectra from frozen solutions were performed as described (Gurbiel et al., 1989; True et al., 1988; Hoffman et al., 1984, 1985).

The first-order ^{14}N ($I = 1$) ENDOR for a single orientation of a paramagnetic center consists, in principle, of four transitions (eq 1). When, as is the case here, $A^N/2 > \nu_N$ and no quadrupolar splittings are resolved, eq 1 describes a two-line Larmor-split pattern centered at $A^N/2$, split by $2\nu_N$. ^{33}S has a nuclear spin, $I = {}^3/_2$, and each magnetically distinct site can give an ENDOR pattern that contains as many as six lines which are centered either at ν_S or at half the hyperfine coupling constant, $A^S/2$, depending on the relative size of these two terms (eq 2). Relaxation effects at Q-band often cause the ν_- feature to be much weaker than its ν_+ partner.

The center of a recorded ENDOR pattern often shifts in the direction of the radio-frequency sweep. The ^{57}Fe hyperfine coupling constants presented in the text are derived by using eq 1 from the spectra shown below, which have been obtained by scanning from high to low radio frequency. They are not accurate because of these shifts. However, the values of the hyperfine parameters presented in Table I are accurate, being the average of values obtained from positive and negative sweeps.

Results

^{57}Fe ENDOR of the $[4Fe\text{-}4S]^+$ Cluster of Reduced Active Enzyme. ^{57}Fe ENDOR experiments have been performed to investigate the $[4Fe\text{-}4S]^+$ cluster of aconitase and its interaction with its substrate; the latter term refers to citrate, isocitrate, or *cis*-aconitate or their mixtures. Earlier we concluded that substrate is bound largely in the form of the dehydrated intermediate *cis*-aconitate under the conditions employed in sample preparation (Telser et al., 1986). Four different types of ^{57}Fe-enriched samples of reduced active enzyme have been studied with ^{57}Fe in either the Fe_a site or the Fe_b sites: substrate-free enzyme, $E(^{57}Fe_a)$ and $E(^{57}Fe_b)$, and the enzyme–substrate complex, $ES(^{57}Fe_a)$ and $ES(^{57}Fe_b)$.

Fe_a Site. ^{57}Fe ENDOR studies of the Fe_a site reveal that it changes dramatically upon binding of substrate. Panels A, B, and C of Figure 2 show the ^{57}Fe ENDOR spectra of $E(^{57}Fe_a)$ obtained by monitoring the EPR signal at positions corresponding to $g_{1,2,3} = 2.06$, 1.93, and 1.86, respectively. In each case, the $I = {}^1/_2$ ^{57}Fe nucleus gives a Larmor-split doublet centered at $A^{Fe}/2$. As the observing g value is moved from g_1 to g_3, the center of the doublet progressively shifts to increasing radio frequency, with the hyperfine coupling increasing from $A(g_1) = 32.8$ MHz to $A(g_3) = 40$ MHz.

The situation is quite different for $ES(^{57}Fe_a)$; Figure 3 shows selected ^{57}Fe ENDOR spectra at various positions across the EPR envelope of $ES(^{57}Fe_a)$ from g_1 to g_3. The single-crys-

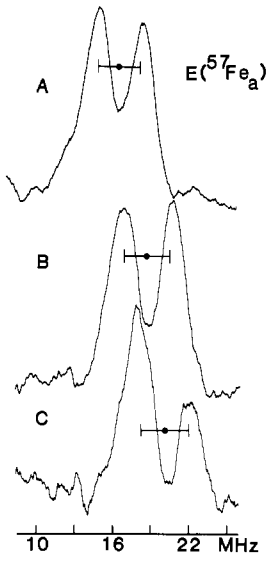

FIGURE 2: ^{57}Fe Q-band (34.61-GHz) ENDOR of Fe_a site in substrate-free enzyme at (A) $g = 2.06$, $H = 1.21$ T; (B) $g = 1.93$, $H = 1.281$ T; and (C) $g = 1.86$, $H = 1.33$ T. The assignment to $A/2$ (●) and twice the Larmor frequency (|—|) are indicated. Conditions: temperature = 2 K; microwave power, 0.08 mW; field modulation, 100 kHz; modulation amplitude, 0.8 mT; rf scan rate, 6 MHz/s; time constant, 0.032 s. The spectra shown have been obtained by scanning from high to low radio frequency.

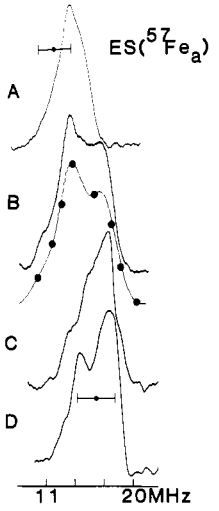

FIGURE 3: ^{57}Fe Q-band (35.06-GHz) ENDOR of Fe_a site in the enzyme–substrate complex at (A) $g = 2.046$, $H = 1.224$ T; (B) $g = 1.94$, $H = 1.29$ T; (C) $g = 1.88$, $H = 1.336$ T; and (D) $g = 1.79$, $H = 1.396$ T. The assignment to $A/2$ (●) and twice the Larmor frequency (|—|) are indicated. A simulated spectrum corresponding to $g = 1.94$ (Figure 2B) using the hyperfine parameter in Table I is shown by the beaded line. Conditions as in Figure 2 except for the following: microwave power, 0.05 mW.

tal-like spectrum taken near g_1 (Figure 3A) shows only a single peak that we assign to ν_+ (eq 1) because of its field dependence; at this field, $2\nu_{Fe} = 3.37$ MHz as shown and the apparent hyperfine coupling from eq 1 is $A(g_1) = 22.5$ MHz, which is only $\sim 2/3$ that for E(^{57}Fe$_a$). As mentioned in the accompanying paper, at Q-band frequency the ν_- resonance is much weaker than ν_+ or is even absent as is the case here. As the observing g value is lowered from g_1 to g_2, anisotropy of the A tensor causes the ν_+ feature to broaden and split into two resolvable features; this splitting is maximal at $g = 1.94$ (Figure 3B). The lower frequency feature of the ν_+ resonance merges with the higher frequency feature for $g \lesssim g_2 = 1.86$ (Figure 3C); in addition, the ν_- resonance begins to grow in intensity and is clearly seen near g_3 (Figure 3D).

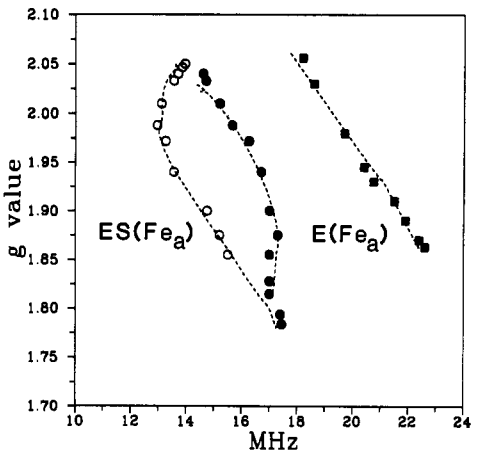

FIGURE 4: ^{57}Fe ENDOR peak position for the ν_+ feature(s) for Fe_a in the substrate-free enzyme (squares) and substrate-bound enzyme (circles) versus the observing g value. Theoretical values calculated by using parameters in Table I are indicated as dashed lines.

Table I: ^{57}Fe Hyperfine Tensors for Fe_a, Fe_{b1}, Fe_{b2}, and Fe_{b3} Sites of the [4Fe-4S]$^+$ Cluster of Aconitase, Substrate Free (E) and in the Enzyme–Substrate (ES) Complex

	principal values and Euler angle[a]	E (ENDOR)	ES (ENDOR)	ES (Mössbauer)[b]
Fe_a	A_1 (MHz)	33	23	26
	A_2 (MHz)	41	32	34
	A_3 (MHz)	42	32	34
	α (deg)	0	25	
Fe_{b3}	A_1 (MHz)	35	35	−32[c]
	A_2 (MHz)	34	42	−39
	A_3 (MHz)	42	43	−39
	α (deg)	0	10	
Fe_{b2}	A_1 (MHz)	27	31	−32[c]
	A_2 (MHz)	34	38	−39
	A_3 (MHz)	37	39	−39
	α (deg)	0	10	
Fe_{b1}	A_1 (MHz)			12
	A_2 (MHz)	25[d] (18)	24[d] (17)	22
	A_3 (MHz)	23[d] (15)	24[d] (17)	12

[a] If we begin with **A** and **g** coaxial, α refers to the rotation of the A tensor about its A_3 axis. [b] Kent et al., 1985. [c] Mössbauer does not distinguish the Fe_{b2} and Fe_{b3} sites. [d] There are two possible interpretations for the Fe_{b1} site; the less favored is placed in parentheses.

Figure 4 shows a plot of the ν_+ ENDOR frequencies as a function of g value for both E(^{57}Fe$_a$) and ES(^{57}Fe$_a$). The solid points represent the experimentally obtained frequencies; the dashed lines are from computer simulations. For E(^{57}Fe$_a$) the smooth variation of ν_+ with g value can be simulated with a nearly axial A tensor that is coaxial with the g tensor. When substrate binds to the enzyme, the A tensor changes dramatically; each of the principal values are reduced by ca. 10 MHz ($\sim 1/3$) and **A** is no longer coaxial with **g**. The principal values of A and the Euler angles that describe its orientation are listed in Table I. Preliminary ^{57}Fe ENDOR measurements of ^{57}Fe$_a$-labeled enzyme with bound nitroisocitrate (Werst, 1990) indicate that the hyperfine coupling for this enzyme–analogue complex is roughly isotropic with $A^{Fe} \sim 30$ MHz, which is comparable to that for substrate-bound enzyme.

Fe_b Sites. The Fe_b sites of the [4Fe-4S]$^+$ cluster have also been studied in both the presence and absence of substrate. In both cases, resonances from three inequivalent iron ions have been observed. In contrast to Fe_a, the hyperfine couplings of the Fe_b sites change very little upon substrate binding. The single-crystal-like (g_1) ^{57}Fe ENDOR spectrum of ES(^{57}Fe$_b$) and E(^{57}Fe$_b$) (Figure 5, panels A and B, respectively) show

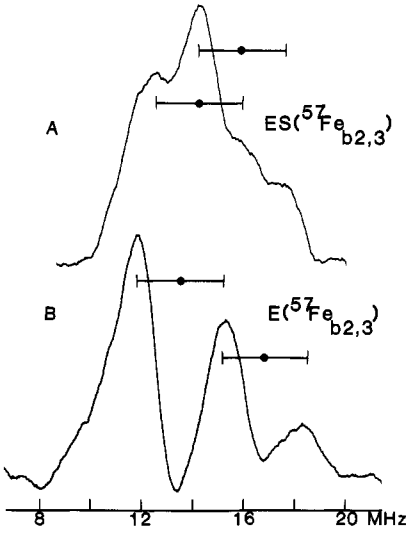

FIGURE 5: ^{57}Fe Q-band ENDOR of Fe_{b2} and Fe_{b3} sites at g_1 in (A) the substrate-free enzyme and (B) the enzyme–substrate complex. Conditions as in Figure 2 except for the following: (A) $g = 2.04$, $H = 1.23$ T; 35.2 GHz; (B) $g = 2.06$, $H = 1.23$ T; 35.37 GHz.

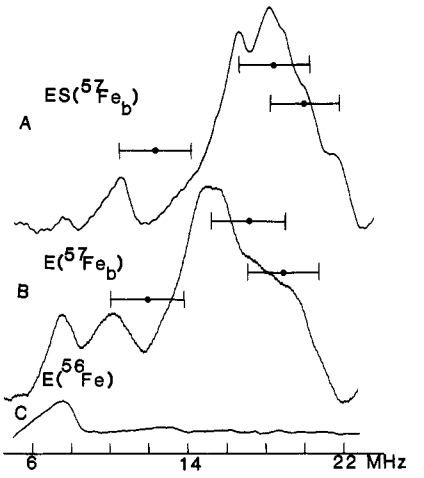

FIGURE 6: ^{57}Fe Q-band ENDOR at g_2 of Fe_b sites in (A) the enzyme–substrate complex, ES($^{57}Fe_b$); (B) the substrate-free enzyme, E($^{57}Fe_b$); and (C) the unenriched, natural abundance E($^{56}Fe_b$) substrate-free enzyme. The solid circles indicate $A^{Fe}/2$ and the bar indicates $2\nu_{Fe}$. Conditions for (A) are as for Figure 2 except for the following: microwave power, 0.05 mW; $g = 1.85$; $H = 1.34$ T; 34.75 GHz. Conditions for panels B and C are as in Figure 2 except for the following: microwave power, 0.125 mW; $g = 1.935$; $H = 1.306$ T; 35.4 6 Hz.

well-resolved resonances due to Fe_{b2} and Fe_{b3}. Note that, at this observing field, the intensity of the ν_- feature of Fe_{b2} and Fe_{b3} in ES($^{57}Fe_b$) and E($^{57}Fe_b$) is considerably greater than the ν_+ feature. The resonances for Fe_{b1} are not seen at this observing g value; they are best observed near g_2 where the resonances for Fe_{b2} and Fe_{b3} occur at higher frequency (Figure 6A,B) and a sharp feature is observed at ca. 10.8 MHz for ES($^{57}Fe_b$) and at ca. 10 MHz for E($^{57}Fe_b$) that can be assigned to Fe_{b1}. The ^{57}Fe ENDOR field dependence (Werst, 1990), suggests that this is the ν_- partner of a doublet with $A^{Fe,b1}(g_2)$ = 25 MHz for ES($^{57}Fe_b$) and $A^{Fe,b1}(g_2)$ = 24 MHz for E($^{57}Fe_b$); however, we cannot rule out the alternative interpretation that it is in fact the ν_+ partner of a signal which would give $A^{Fe,b1}(g_2)$ = 18 MHz for ES($^{57}Fe_b$) and $A^{Fe,b1}(g_2)$ = 17 MHz for E($^{57}Fe_b$). The signal seen at ~8 MHz in the spectra of E(^{57}Fe) (Figure 6B) and E(^{56}Fe) (Figure 6C) is due to endogenous nitrogen and will be discussed in a later section.

The principal values and orientation of the ^{57}Fe A tensors for the Fe_{b2} and Fe_{b3} sites of E($^{57}Fe_b$) and ES($^{57}Fe_b$) have been obtained by analyzing the spectra taken at selected g values across the EPR envelope and are summarized in Table I. The resonances from the Fe_{b1} site are seen only over a limited range of the EPR spectrum; the hyperfine parameters of this site could not be fully analyzed, but estimates of A_2 and A_3 values have been made. Because there are two possible interpretations for the Fe_{b1} signals, the estimates of A_2 and A_3 are listed in Table I with the less favored values placed in parentheses. The values obtained for the Fe_b sites of ES($^{57}Fe_b$) from Mössbauer studies are also shown in Table I.

Calculation of Spin-Coupling Parameters. The ^{57}Fe hyperfine couplings of the four iron ions, i, reported in Table I, $A(i)$, are defined in terms of the nuclear-spin interaction with the total electron spin of the spin-coupled [4Fe-4S]$^+$ cluster. However, the coupling for Fe_i arises from a nuclear hyperfine interaction with the isolated local spin ($^5/_2$ for Fe^{3+}; 2 for Fe^{2+}) on that site having a coupling constant $a(i)$; the two parameters are proportional:

$$A(i) = K(i)\, a(i) \qquad (3)$$

To analyze the ^{33}S ENDOR data presented below, we must determine the proportionality factor, $K(i)$, for each cluster iron. This can be done by using the local-spin matrix elements if the spin coupling scheme is known, as for a [2Fe-2S] cluster (Gibson et al., 1966), or it can be done by solving equations generated by a spin-coupling scheme, as in the case of the [3Fe-4S]$^+$ cluster of *Desulfovibrio gigas* ferredoxin II (Kent et al., 1980). However, because the coupling scheme is not known for the [4Fe-4S]$^+$ cluster, we use an alternative technique that is adequate for our purposes; rearranging eq 3, we estimate $K(i)$ as the ratio of the observed values for the isotropic ^{57}Fe coupling for site i within the cluster, $A_{iso}(Fe_i)$, namely, 1/3 the trace of this site's tensor listed in Table I, to the isotropic coupling for an isolated Fe^{3+} or Fe^{2+} site in rubredoxin (Kent & Huynh, 1984), $a(Fe^{3+})$ and $a(Fe^{2+})$, respectively.

The Mössbauer quadrupole and isomer shifts indicate that the Fe_{b2} and Fe_{b3} sites of the [4Fe-4S]$^+$ cluster are "ferric type" (charge +2.5) sites whereas the Fe_{b1} and Fe_a sites are ferrous in character (Kent et al., 1985). For the [4Fe-4S]$^+$ cluster of ES the data in Table I give $A_{iso}(Fe_a)$ = 29 MHz, $A_{iso}(Fe_{b2})$ = −36 MHz, and $A_{iso}(Fe_{b3})$ = −40 MHz, and the Mössbauer data for the Fe_{b1} site give $A_{iso}(Fe_{b1})$ = +15 MHz. Taking $a(Fe^{3+})$ = −23 MHz and $a(Fe^{2+})$ = −27 MHz, respectively (Kent & Huynh, 1984), we obtain the following: $K(Fe_a)$ = −1.1, $K(Fe_{b1})$ = −0.6, $K(Fe_{b2})$ = +1.6, and $K(Fe_{b3})$ = +1.7.

Similarly, for the [4Fe-4S]$^+$ cluster of substrate-free enzyme, E, the data in Table I give $A_{iso}(Fe_a)$ = 39 MHz, $A_{iso}(Fe_{b2})$ = −33 MHz, and $A_{iso}(Fe_{b3})$ = −37 MHz. The hyperfine coupling tensor for Fe_{b1} is incompletely determined from ENDOR and cannot be determined from Mössbauer; however, we note that the addition of substrate causes little change in the hyperfine values for the Fe_b (Table I) and make the approximation that $A_{iso}(Fe_{b1})$ = +15 MHz as found from the Mössbauer data for ES. Calculation for E with eq 3 yields the following: $K(Fe_{ca})$ = −1.4, $K(Fe_{b1})$ = −0.6, $K(Fe_{b2})$ = 1.4, and $K(Fe_{b3})$ = 1.6.

^{33}S ENDOR. ENDOR spectra of substrate-bound ^{33}S-enriched [4Fe-4S]$^+$ reduced active aconitase, ES(^{33}S), exhibit features in the range 3–12 MHz that are not present in the spectrum of ES(^{32}S). Figure 7 shows spectra obtained by monitoring the g_1, g_2, and g_3 signals, respectively. ^{33}S has a nuclear spin $I = {}^3/_2$, and according to eq 1, each magnetically distinct site can give a doublet pattern centered either at ν_S or at A^S, depending on the relative size of these two terms,

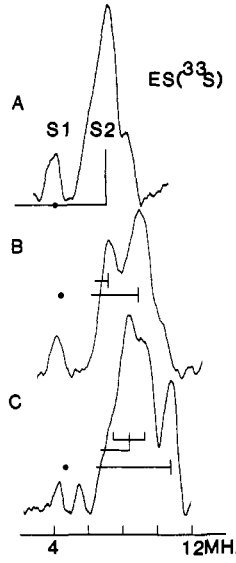

FIGURE 7: ^{33}S ENDOR at Q-band (34.76 GHz) of the [4Fe-4S]$^+$ form of the enzyme with bound substrate: (A) g = 2.04, H = 1.218 T; (B) g = 1.85, H = 1.339 T; (C) g = 1.786, H = 1.386 T. The solid circle represents ν_S, and the bars indicate possible assignments of hyperfine (A–C) and quadrupole (C) splittings for the S2 sulfides. Conditions are as in Figure 2 except for the following: microwave power, 0.05 mW.

with the ν_+ and ν_- features each exhibiting as many as three lines. In the case of ^{33}S-enriched aconitase, with its four $^{33}S^{2-}$ ions, there could be as many as 24 lines in a single-crystal-like spectrum. However, the single-crystal like spectrum taken near g_1 (Figure 7A) is much simpler than this. It shows an intense feature at ca. 7 MHz that can be assigned to the ν_+ signal of a pattern centered at ν_S = 3.98 MHz and corresponding to A(S1) $\approx$ 6 MHz; the ν_- signals would be at low radio frequency, ca. 1 MHz, where the signal intensity is too weak to be observed. The low-frequency and high-frequency shoulders of this feature are attributable to quadrupolar interactions with the $I = {}^3/_2$, ^{33}S nucleus (P = 0.9 MHz), and/or to a slight inequivalence between similar ^{33}S sites. Such ambiguity is associated with most spectra; for example, at g_2 (Figure 7B) the strong signals seen at 7 and 9 MHz can be assigned to two inequivalent sulfur sites (A = 5.5 MHz and A = 8.6 MHz) but might arise from splittings seen at this non-single-crystal orientation. However, the single-crystal-like spectrum taken at g_3 (Figure 7C) appears to be best assigned to two types of ^{33}S sites. The intense peak at ~8 MHz is assigned to one sulfur with A = 7.6 MHz; as shown, the additional structure on this peak can be attributed to resolved quadrupolar interaction, P = 0.7 MHz. The well-resolved signal at ca. 11 MHz is assigned to a second type of ^{33}S site (A = 12.6 MHz). In addition to these signals with $A^S > 6$ MHz, there are weak ^{33}S signals centered near ν_S for each of the three spectra shown here. These resonances are assigned to sulfur sites that are weakly interacting (A $\lesssim$ 1 MHz).

The field dependence of the ^{33}S resonances thus suggests that there are two types of S^{2-} sites, one that most likely corresponds to two sulfides with roughly isotropic hyperfine couplings in the range 6–12 MHz, and the other, to the remaining S^{2-}, which have small couplings, A $\lesssim$ 1 MHz. By analyzing the observed hyperfine parameters in terms of the spin coupling within the [4Fe-4S]$^+$ cluster, we support this suggestion by showing that the four bridging S^{2-} ions are expected to fall into two pairs, one with relatively large A^S and the other with A^S approaching zero. The analysis further locates these pairs within the [4Fe-4S]$^+$ cube relative to the iron sites.

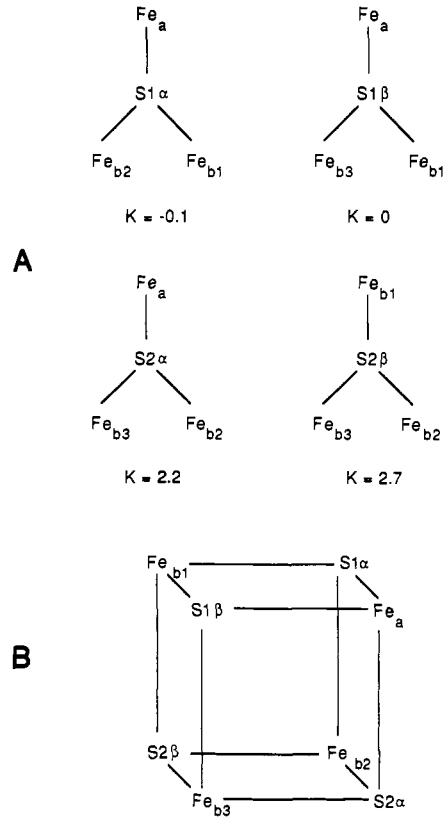

FIGURE 8: (A) Representation of the four S^{2-} sites of the [4Fe-4S]$^+$ cluster in the enzyme–substrate complex, each with its three neighboring iron sites; $K = K$(neighbors), eq 5, is shown for each site. (B) Relative positions of S^{2-} and Fe sites within cluster cube.

Each S^{2-} ion of the [4Fe-4S]$^+$ cluster is bonded to three neighboring iron ions; for S^{2-} ion k, we adopt a generalized form of eq 3 for $A(S_k)$, the observed ^{33}S coupling constant associated with the *total* spin $S = {}^1/_2$ of the spin-coupled cluster:

$$A(S_k) = \sum_i A(S_k,i) = \sum[K(i)\ a(S_k,i)] \qquad (4)$$

where the $a(S_k,i)$ in eq 4 represent the superhyperfine coupling to the individual *local* spins of the three adjacent iron ions, i, and the $K(i)$ have been determined above. As a first approximation, we further adopt a single value for the intrinsic sulfur interaction constants, $a(S_k,i) = a$(S), which gives as a subcase of eq 4

$$A(S_k) = [\sum K(Fe_i)][a(S)] \equiv K(\text{neighbors})\ a(S) \qquad (5)$$

Hence the observed hyperfine coupling constant for an individual S^{2-} ion appears as a simple sum of the contributions from its three neighboring iron ions. Figure 8 illustrates the dependence of the resulting sum on the location of the S^{2-} ion within the cube: $K(Fe_a,Fe_{b1},Fe_{b2})$ = −0.1; $K(Fe_a,Fe_{b1},Fe_{b3})$ = 0; $K(Fe_a,Fe_{b2},Fe_{b3})$ = 2.2; $K(Fe_{b1},Fe_{b2},Fe_{b3})$ = 2.7. Thus, this simplified analysis predicts that the four sulfur sites will fall into two categories, two with negligible hyperfine couplings, $K \sim$ −0.1–0, and two with appreciable couplings, $K \sim$ 2–3. This correlates well with the observed ^{33}S hyperfine couplings which also fall into two classes, $A_S \sim$ 6–12 MHz and $A_S \sim$ 0–1 MHz. The analysis gives a(S) $\sim$ 2–4 MHz. To indicate just how small this value is, note that one electron in a 3s orbital on sulfur is predicted to give an isotropic coupling of a_0(S) $\sim$ 3500 MHz (Morton & Preston, 1978).

ENDOR spectra of E(^{33}S) show resonances between 6.5 and 11 MHz that do not appear in the spectrum of the E(^{32}S) control. Figure 9 shows the ν_+ resonances (eq 1) in ^{33}S EN-

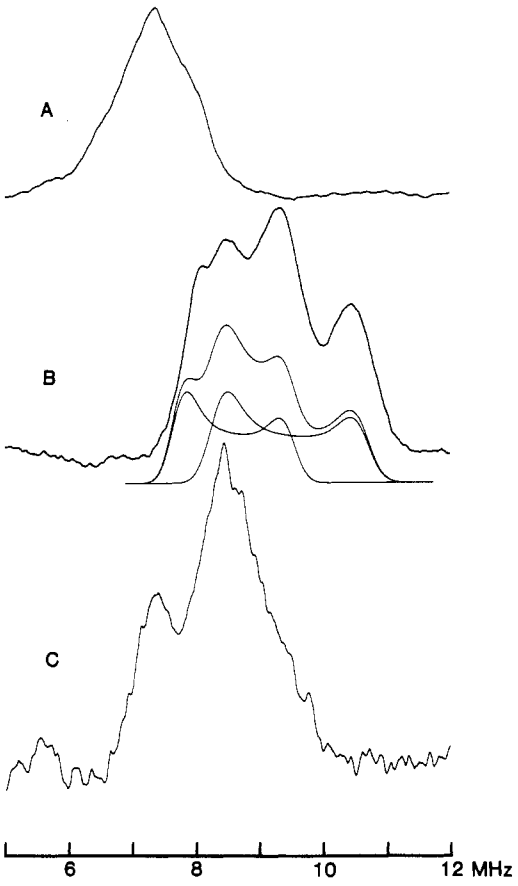

FIGURE 9: ^{33}S ENDOR at Q-band (34.55 GHz) of the [4Fe-4S]$^+$ form of E(^{33}S): (A) g = 2.04, H = 1.21 T; (B) g = 1.93, H = 1.28 T; (C) g = 1.85, H = 1.335 T. The simulation below spectrum B shows individual contributions from the two types of S^{2-} ions, along with their sum. Hyperfine tensors employed are given in the text; line width and intensities were adjusted visually. Conditions: temperature = 2 K; microwave power, 0.05 mW; field modulation, 100 kHz; modulation amplitude, 0.8 mT; rf scan rate, 0.75 MHz/s; time constant, 0.064 s. Spectrum A was scanned from high to low radio frequency; spectra B and C were scanned from low to high. Consequently, for direct comparisons, spectrum A should be shifted ca. 1 MHz toward higher frequency. (See Procedures and Theory.)

DOR spectra taken at g_1, g_2, and g_3. The ν_- feature would again be at low radio frequency and would be undetectable. The ν_+ feature in the single-crystal-like spectrum at g_1 (Figure 9A) is centered at ~8.5 MHz, corresponding to A(S) ~ 6.5 MHz. The spectrum at g_3 consists of two peaks also centered at ~6.5 MHz and is interpretable as arising from at least two types of S^{2-} ions, one with A(S) ~ 8.5 MHz and one with A(S) ~ 6.3 MHz. The spectrum at g_2 has four discernible peaks (Figure 9B). Three of these have remained near ν ~ 8.5 MHz; one peak has moved to higher frequency as a result of hyperfine anisotropy and gives $A(g_2)$ ~ 12 MHz. Because we do not see any resonances near ν_S, it is plausible that the resonances of all four S^{2-} ions are contained in the features of Figure 9, unlike those for ES; furthermore, EPR simulations show that there can be no ^{33}S sites that have appreciably larger hyperfine couplings, but undetected ENDOR signals. We find that the full field dependence of the ENDOR spectra (Figure 9 plus other data), including the resolved spectrum at g_2, can be simulated by assuming that there are two types of S^{2-} ions that have no resolved quadrupole splittings; one has a hyperfine tensor $A(S1)_{1,2,3}$ ~ [6.8, 10.1, 6.5] MHz, and the other has the tensor $A(S2)_{1,2,3}$ ~ [6.3, 12.4, 8.7] MHz. A simulation for the spectrum at g_2 is presented in Figure 9. These tensors can be decomposed into their isotropic parts A(S1) = 7.8 and A(S2) = 9.1 MHz and anisotropic components that reflect spin density in the 3p orbitals of sulfur.[1]

We can apply to E the analyses based on eq 4 and 5, as done for ES. We find the following: $K(Fe_a,Fe_{b1},Fe_{b2})$ = −0.6, $K(Fe_a,Fe_{b1},Fe_{b3})$ = −0.4, $K(Fe_a,Fe_{b3},Fe_{b2})$ = 1.6, and $(Fe_{b1},Fe_{b2},Fe_{b3})$ = 2.4. Comparison with the values for ES gives the qualitative impression that the ^{33}S hyperfine couplings in E should also fall into two classes, but not as cleanly, and that the smallest hyperfine values should not be as near A = 0. We can readily accommodate the assignment that the four S^{2-} behave as two types whose resonances appear in Figure 9 by allowing for variations in the $a(S_k,i)$ (eq 4 instead of eq 5), as expected from theoretical calculations (Noodleman, 1988). In this analysis the two observed A(S) could arise in a number of ways, depending on the sites involved and on the number of sulfides in each of the two classes. In any case this would give $a(S_k,i)$ in the range ~2–17 MHz. Similarly, the hyperfine anisotropy[1] would have intrinsic values of ~0.5–3 MHz, depending on the site involved. Note that this analysis gives $a(S_k,i)$ for E that are substantially larger than those for ES, but that the values for ES still are small compared to a_0(S). The anisotropy is likewise small compared to that for one electron in a 3p orbital on sulfur (~200 MHz; Morton & Preston, 1978) and would correspond to a net spin delocalization to S^{2-} of ≲1% per interacting iron ion.

^{14}N ENDOR of the [4Fe-4S]$^+$ Cluster. ENDOR spectra of natural abundance E(^{56}Fe) (Figure 6C) and ES(^{56}Fe) (not shown) taken at Q-band shows a resonance at ca. 8 MHz that we assign to the ν_+ branch of a ^{14}N ENDOR pattern, giving A(N1) = 7 MHz for E(^{56}Fe) and A(N1) = 6.8 MHz for ES(^{56}Fe). The corresponding ν_- features would be expected at low radio frequency, at ~1 MHz where the signal intensity is too low to be detected.

The ENDOR field dependence of the ^{14}N resonance of E and ES (not shown) indicates that the ^{14}N hyperfine interaction of E and ES is roughly isotropic. This indicates the nitrogen covalently interacts with the cluster. The principal values of the ^{14}N hyperfine tensor in the substrate-free enzyme, E, are almost identical with the values for the enzyme–substrate complex, ES. Because substrate binding dramatically affects the Fe_a site, these ENDOR results suggest that the ^{14}N resonances are associated with the [3Fe-4S]$^+$ portion of the cluster. Hence, in attempting to analyze these resonances as done for ^{33}S, we need consider only those interactions that involve the Fe_b sites, namely, a situation where nitrogen is ligated to Fe_b sites or interacts through hydrogen bonds with the Fe_b sites via the terminal sulfur or with the unique sulfide that bridges the Fe_{b1}, Fe_{b2}, and Fe_{b3} site. As discussed elsewhere (Werst, 1990), the magnitude of A(N) is consistent with an intrinsic, local-spin coupling of 3.5 < a(N) < 16 MHz, depending on which type of interaction is assumed.

The breadth of the range does not permit a conclusion as to whether the nitrogen is a ligand to iron. However, the crystal structure of the [3Fe-4S]$^+$ form of the pig heart aconitase indicates that the cluster ligand provided by the protein to each of the three Fe_b sites is a cysteine (Robbins & Stout, 1989). This leads us to interpret the ^{14}N interaction as being due to NH···S bonds. The aconitase structure shows two

[1] The anisotropic component of the S1 tensor has roughly axial symmetry, $T(S1)_{1,2,3} \approx$ [−1.0, 2.3, −1.3] MHz, as expected for spin density in a 3p orbital (Atherton, 1974). That of the S2 tensor is [−2.8, 3.3, −0.4]. The S2 tensor can be decomposed into two axial components in three ways. One way gives $T(S2)_{1,2,3}$ = [−2.0, 4.1, −2.0] + [−0.8, −0.8, 1.6] MHz (uncertainty ±0.5 MHz), corresponding to spin density in two orthogonal 3p orbitals. For discussion, the anisotropy of an axial tensor is measured by a parameter, T, such that the unique axis has value 2T, i.e., $T(S1)_{1,2,3}$ = [−T, 2T, −T].

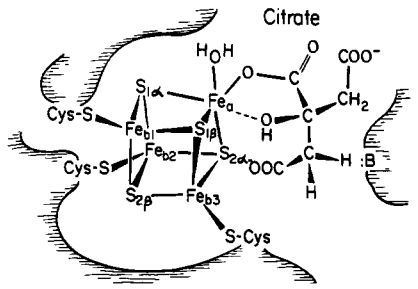

FIGURE 10: Representation of ENDOR-derived information about the [4Fe-4S]$^+$ cluster of the aconitase enzyme–substrate complex, showing the two pairs of sulfur, S1α, S1β and S2α, S2β, in relationship to the four inequivalent iron sites, Fe_a, Fe_{b1}, Fe_{b2}, and Fe_{b3}, along with the bound substrate.

bridging sulfurs and one Cys sulfur of the cluster are within 3.0, 3.6, and 3.6 Å, respectively, of main-chain amide nitrogens that make appropriate angles to form N–H···S bonds and further shows several histidyl imidazole residues in close proximity to the cluster. This interpretation predicts that there should be a proton with substantial isotropic hyperfine couplings and furthermore that this proton should be exchangeable under appropriate conditions. Preliminary attempts to detect resonances from the hydrogen of the proposed NH···S bonds of aconitase by deuterium exchange reactions have yielded negative results. In one experiment apoaconitase was cyanolysed at pH 9.0 in the presence of ^2H_2O and then reconstituted in ^2H_2O to yield active enzyme. In another, aconitase was converted to purple aconitase at pH 10.5 in ^2H_2O and then reconverted to active enzyme. In neither case were deuterium ENDOR signals observed, nor was there any loss of the usual proton signals as determined by ^{1}H ENDOR.[2] However, these results are not conclusive since the conditions used might not have been suitable for exchange.

Discussion

^{57}Fe ENDOR. The ENDOR measurements described here have allowed us to characterize the substrate-free and substrate-bound [4Fe-4S]$^+$ forms of aconitase by ^{57}Fe, ^{14}N, and ^{33}S ENDOR spectroscopy. The ^{57}Fe ENDOR data clearly show that all four iron sites of the [4Fe-4S]$^+$ cluster are inequivalent in both the substrate-free enzyme and the enzyme–substrate complex.

The resonances of Fe_a, Fe_{b2}, and Fe_{b3} can be followed at all positions across the EPR envelope: as a result, for the A tensors of these sites we have obtained the principal values and orientations with respect to the g tensor (Table I). Only one branch of the signal from the Fe_{b1} can be resolved at any given g value, and this signal only in a limited range of g values, g_2 to g_3. Hence the full set of hyperfine parameters could not be obtained for Fe_{b1} (Table I). Mössbauer spectra of the enzyme–substrate complex do not distinguish the Fe_{b2} and Fe_{b3} sites and were therefore analyzed in terms of three types of sites, Fe_a, and two types of Fe_b sites, Fe_{b1} and $Fe_{b2,3}$, present in the ratio 1:2 (Table I); moreover, the Mössbauer technique is insensitive to the relative orientation of the g and A tensors. However, Mössbauer measurements performed in a strong applied magnetic field provided the sign of the hyperfine coupling, showing that Fe_a and Fe_{b1} have A tensors with positive components whereas Fe_{b2} and Fe_{b3} have A tensors with negative components.

^{17}O ENDOR studies have shown that substrate binding involves coordination of a single substrate carboxyl group [Kennedy et al., 1987; Werst et al., 1990 (accompanying paper)]. The coordination site is Fe_a, which is dramatically affected by substrate binding; this is reflected in the hyperfine tensor of Fe_a through changes both in its principal values and orientation with respect to the g tensor. It is also seen in Mössbauer studies: significant changes in the isomer shift of Fe_a when substrate is bound are consistent with Fe_a becoming 5- or 6-coordinate instead of 4-coordinate as in the substrate-free species. The perturbations caused by binding a carboxyl group to Fe_a (Werst et al., 1990) are quite localized: The ^{57}Fe hyperfine values listed in Table I show that the properties of the other three iron sites, $Fe_{b1,2,3}$, are largely insensitive to substrate binding.

Analysis of ^{33}S resonances from the [4Fe-4S]$^+$ cluster of the enzyme–substrate complex suggests that the sulfur sites occur as two pairs, one with $A^S \sim 6$–12 MHz and another with $A^S \lesssim 1$ MHz. The spatial relationship of these pairs with respect to the iron sites is given in Figure 8. The analysis indicates that the intrinsic hyperfine interaction constant for S^{2-} bonded to an iron ion in the cluster is extremely small, $a(S) \sim 2$–4 MHz. The ^{33}S ENDOR results for the enzyme without substrate are not qualitatively different. They also can be interpreted in terms of two types of sites with $a(S) \lesssim 17$ MHz; in addition, the sulfides exhibit anisotropic couplings that are equivalent to $\lesssim 1\%$ spin delocalization to S^{2-} 3p orbitals per neighboring iron ion. Thus, one can firmly state that the Fe–S bonding within the cluster gives rise to remarkably small spin density on sulfur.

Attempts to observe ^{77}Se resonances from reconstituted protein have not been successful, presumably because of interference by ^{14}N resonances such as those we have observed with the [4Fe-4S]$^+$ cluster and have interpreted as arising from hydrogen bonds between NH groups of the protein and bridging or terminal sulfur sites of the Fe-S cluster. These observations will be further pursued by comparison to other Fe-S proteins.

In conclusion, Figure 10 summarizes relevant aspects of the current structural information about the active site of the aconitase ES complex. The X-ray diffraction structure of Robbins and Stout (1989) shows cysteines 358, 421, and 424 bound to the three Fe_b sites, although the correspondence is not known. The exogenous ligands to Fe_a are indicated by ENDOR to be H_2O and carboxyl of substrate; depending on the state, hydroxyl of substrate also may bind (as inferred from nitroisocitrate; see preceding paper in this issue). Finally, the relative disposition within the cube of sulfide and iron ions as deduced here (Figure 8) is included. The structural features indicated in Figure 10 have led to substantial improvements in our understanding of aconitase function [see Emptage (1988) and Beinert and Kennedy (1989)].

Acknowledgments

We acknowledge the use of the EPR facilities at the National Biomedical ESR Center (supported by National Institutes of Health Grant RR 01008) and of preparative facilities at the Institute for Enzyme Research, University of Wisconsin, Madison.

Registry No. Aconitase, 9024-25-3.

References

Abragam, A., & Bleaney, B. (1970) *Electron Paramagnetic Resonance of Transition Ions*, Clarendon, Oxford.

Atherton, N. M. (1974) *Electron Spin Resonance*, Wiley, New York.

Beinert, H., & Kennedy, M. C. (1988) *Eur. J. Biochem. 186*, 5–15.

[2] Added in proof: ENDOR results of more recent H/D exchange experiments show weakly coupled deuteron resonances.

Brauer, G. (1963) *Handbook of Preparative Inorganic Chemistry*, Vol. 1, pp 358–360, Academic Press, New York.
Emptage, M. H. (1988) in *ACS Symposium Series* (Que, L., Jr., Ed.) No. 372, pp 343–371, American Chemical Society, Washington, DC.
Gibson, J. F., Hall, D. O., Thornley, J. H. M., & Whatley, F. R. (1966) *Proc. Natl. Acad. Sci. U.S.A. 56*, 987–990.
Gurbiel, R. J., Batie, C. J., Sivaraja, M., True, A. E., Fee, J. A., Hoffman, B. M., & Ballou, D. P. (1989) *Biochemistry 28*, 4861–4871.
Hoffman, B. M., Martinsen, J., & Venters, R. A. (1984) *J. Magn. Reson. 59*, 110–123.
Hoffman, B. M., Martinsen, J., & Venters, R. A. (1985) *J. Magn. Reson. 62*, 537–542.
Kennedy, M. C., Werst, M., Telser, J., Emptage, M. H., Beinert, H., & Hoffman, B. M. (1987) *Proc. Natl. Acad. Sci. U.S.A. 84*, 8854–8858.
Kent, T. A., & Huynh, B. H. (1984) *Advances in Inorganic Biochemistry* (Marzilli, L. G., & Eichhorn, G. L., Eds.) Vol. 6, pp 163–233, Elsevier, Amsterdam.
Kent, T. A., Huynh, B. H., & Munck, E. (1980) *Proc. Natl. Acad. Sci. U.S.A. 77*, 6574–6576.
Morton, J. R., & Preston, K. F. (1978) *J. Magn. Reson. 30*, 577–582.
Münck, E. (1985) *J. Biol. Chem. 260*, 6371–6381.
Noodleman, L. (1988) *Inorg. Chem. 27*, 3677–3679.
Robbins, A. H., & Stout, C. D. (1989a) *Proc. Natl. Acad. Sci. U.S.A. 86*, 3639–3643.
Robbins, A. H., & Stout, C. D. (1989b) *Proteins: Struct., Funct., Genet. 5*, 289–312
Surerus, K. K., Kennedy, M. C., Beinert, H., & Münck, E. (1989) *Proc. Natl. Acad. Sci. U.S.A. 86*, 9846–9850
Telser, J., Emptage, M. H., Merkle, H., Kennedy, M. C., Beinert, H., & Hoffman, B. M. (1986) *J. Biol. Chem. 261*, 4840–4846.
True, A. E., Nelson, M. J., Venters, R. A., Orme-Johnson, W. H., & Hoffman, B. M. (1989) *J. Am. Chem. Soc. 110*, 1935–1943.
Venters, R. A., Nelson, M. J., McLean, P., True, A. E., Levy, M. A., Hoffman, B. M., & Orme-Johnson, W. H. (1986) *J. Am. Chem. Soc. 108*, 3487–3498.
Werst, M. M. (1990) Ph.D. Thesis, Northwestern University.
Werst, M. M., Kennedy, M. C., Beinert, H., & Hoffman, B. M. (1990) *Biochemistry* (preceding paper in this issue).

Occurrence and Significance of Diastereomers of Methotrexate α-Peptides†

Ulrike Kuefner,‡ Angelika Esswein,§ Ute Lohrmann, Yolanda Montejano, Karin S. Vitols, and F. M. Huennekens*
Division of Biochemistry, Department of Molecular and Experimental Medicine, Research Institute of Scripps Clinic, La Jolla, California 92037

Received June 6, 1990; Revised Manuscript Received August 8, 1990

ABSTRACT: The L,L diastereomer of methotrexate-α-alanine (L,L-MTX-Ala) was synthesized by reaction of α-L-glutamyl-L-alanine di-*tert*-butyl ester with 4-amino-4-deoxy-10-methylpteroic acid, followed by removal of the blocking groups. It was identified by HPLC (C_{18} reversed-phase silica gel; acetic acid/CH_3OH) as the slower of two closely spaced components in DL,L-MTX-Ala prepared previously by a different route [Kuefner et al. (1989) *Biochemistry 28*, 2288–2297]. The L,L diastereomer was hydrolyzed by pancreatic carboxypeptidase A (to yield MTX and Ala) twice as rapidly as the DL,L mixture. Analysis of the latter by HPLC established that the slower component was hydrolyzed to MTX and that the unreactive, faster component was D,L-MTX-Ala. DL,L-MTX-Arg was resolved by HPLC (NH_4OAc/CH_3CN) into two closely spaced components, and the diastereomers were partially separated by chromatography on DEAE-Trisacryl ($H_2O \rightarrow 2\%$ NH_4HCO_3). Serum carboxypeptidase N hydrolyzed only the slower HPLC component (to yield MTX and Arg), thereby identifying it as the L,L diastereomer. When tested for cytotoxicity against L1210 cells, L,L-MTX-Arg ($ID_{50} = 1.6 \times 10^{-8}$ M) was more effective than the D,L diastereomer ($ID_{50} = 2.2 \times 10^{-7}$ M). Treatment of MTX with dicyclohexylcarbodiimide and *N*-hydroxysuccinimide (NHS), followed by hydrolysis of the NHS ester, led to racemization in the L-glutamate moiety of MTX as shown by the fact that the product was hydrolyzed by carboxypeptidase G_2 (at the pteroate–Glu bond) only to the extent of ca. 50% compared to the untreated control. These observations have a broad significance, since coupling agents are employed extensively in the derivatization of MTX for attachment to affinity supports and monoclonal antibodies.

Previous studies from this laboratory (Kuefner et al., 1988, 1989) have demonstrated that methotrexate α-peptides (i.e., derivatives in which amino acids are joined via an amide linkage to the α-carboxyl group of MTX[1]) can be hydrolyzed by carboxypeptidases to yield MTX; MTX-α-alanine (MTX-Ala) and MTX-α-arginine (MTX-Arg), for example, were substrates for pancreatic CP-A and serum CP-N, respectively. The MTX peptides were relatively nontoxic, presumably because derivatization of the α-carboxyl suppresses cellular uptake of the drug (Sirotnak et al., 1979). These results suggested that MTX peptide/carboxypeptidase combinations,

† Supported by an Outstanding Investigator Grant (CA-39836) from the National Cancer Institute, National Institutes of Health, and by a grant (CH-31Z) from the American Cancer Society. Manuscript 5662-BCR from the Research Institute of Scripps Clinic.

* Author to whom correspondence should be addressed.
‡ Recipient of a Postdoctoral Fellowship from the Deutsche Forschungsgemeinschaft. Present address: Abteilung Pharmachemie, Boehringer Ingelheim KG, D-6507 Ingelheim, West Germany.
§ Present address: Abteilung Therapeutika, Boehringer Mannheim GmbH, D-6800, Mannheim, West Germany.

[1] Abbreviations: MTX, methotrexate; MTX-Ala and -Arg, peptides in which the indicated amino acids are linked covalently to the α-COOH of MTX; CP-A, -N, and -G_2, carboxypeptidases A, N, and G_2; DCC, *N*,*N*′-dicyclohexylcarbodiimide; NHS, *N*-hydroxysuccinimide; DMF, dimethylformamide; ID_{50}, concentration producing 50% inhibition of cell growth.

0006-2960/90/0429-10540$02.50/0